A&A 660, A49 (2022)
https://doi.org/10.1051/0004-6361/202142111

Astronomy & Astrophysics

New exocomets of β Pic

Ya. Pavlenko[1,2], I. Kulyk[1], O. Shubina[1,3], M. Vasylenko[1], D. Dobrycheva[1], and P. Korsun[1]

[1] Main Astronomical Observatory of the NAS of Ukraine, 27 Akademika Zabolotnoho Str., 03143 Kyiv, Ukraine
e-mail: yp@mao.kiev.ua
[2] Centre for Astrophysics Research, University of Hertfordshire, College Lane, Hatfield AL10 9AB, UK
[3] Astronomical Observatory of Taras Shevchenko National University of Kyiv, 3 Observatorna Str., 04053 Kyiv, Ukraine

Received 30 August 2021 / Accepted 25 February 2022

ABSTRACT

Aims. The aim of our work is to analyze the light curves of β Pic which were recently observed by the Transiting Exoplanet Survey Satellite (TESS) in sectors 32, 33, and 34 by searching for the signatures of exocomet transits.
Methods. We processed the β Pic light curves from the Mikulski Archive for Space Telescopes database, applying the frequency analysis to remove harmonic signals due to the star's pulsations, and we used a simple 1D model to fit the profiles of the events that were found.
Results. We recovered events previously found by other authors in sectors 5 and 6 and found five new distinct aperiodic dipping events with asymmetric shapes resembling the expected profiles due to the passage of a comet-like body across the star disk. These dips are rather shallow, with the flux drop at a level of 0.03% and a duration of less than 1 day. No periodic transits were found in the sectors investigated.
Conclusions. The depth and duration of the identified dips are similar to the recently discovered transits in the β Pic light curves from sector 5 of the TESS observations as well as to those found in the light curves of KIC 354116 and KIC 1108472 from the *Kepler* database. This indicates that aperiodic shallow dips are not likely an exceptional phenomenon, at least for the β Pic system.

Key words. binaries: general – stars: individual: β Pictoris – planetary systems – methods: data analysis – comets: general

1. Introduction

β Pic belongs to the β Pic moving group, a kinematic group of stars in the vicinity of the Solar System (Zuckerman & Song 2004). The age of the group population is estimated in the range from about 10 Myr to 40 Myr with a medium consensus age of 23 ± 3 Myr (Mamajek & Bell 2014). β Pic is a young A5V star with a mass of about 1.7–1.8 $M_{\odot}$, which is already evolved to be at the zero age main sequence (ZAMS) or on the ZAMS (Crifo et al. 1997). The significant excess in the infrared (IR) emissions observed by the Infrared Astronomical Satellite (IRAS) reveals the existence of dust shells around β Pic (Backman et al. 1986; Cote 1987). Successive models of the IR emitting region around β Pic suggest its complex architecture, which is confirmed by direct imaging of the ring features and the discovery of two planets β Pic b and β Pic c, embedded in the disk (Smith & Terrile 1984; Kalas et al. 2000; Wahhaj et al. 2003; Lagrange et al. 2020). Indirect evidence for the existence of a minor body population, planetesimals, and/or cometesimals in the β Pic system was obtained by discovering falling evaporating bodies (FEBs), which manifest themselves as the strong redshifted variations in the profiles of the circumstellar absorption lines. These variable spectral features can be associated with comet-like bodies in the star-grazing orbits falling on the parent star (Ferlet et al. 1987; Beust et al. 1996). The redshifted spectral components can be divided into two distinct classes: low velocity and high velocity features. The former ones are usually deep, and their redshift velocities with respect to the central component fall between 10–20 km s^{-1} and 50 km s^{-1}. The latter ones appear to be shallower, varying on a shorter timescale. Their typical redshifts are about 100 km s^{-1} (Beust et al. 1998). A strong transient blueshifted feature was also found in the circumstellar Ca II K line shifted by 14 km s^{-1} with respect to the "stable," circumstellar component at a velocity of 22 km s^{-1} (Lagrange-Henri et al. 1988; Crawford et al. 1998). The blueshifted feature implies the existence of a comet-like object on a significantly different orbit from those causing the redshifted variations (Kiefer et al. 2014). The short-term optical variation of the β Pic brightness was first reported by Lecavelier Des Etangs et al. (1995). To explain the phenomenon, the mechanism of the star's light scattering by an elongated dust cloud or by a cometary coma passing across the star's disk was adopted as the most plausible one (Lamers et al. 1997). Recently, Zieba et al. (2019) presented the β Pic light curve analysis based on the Transiting Exoplanet Survey Satellite (TESS) data. They found three transit events interpreted as exocomet passages across the stellar disk of β Pic. The purpose of this paper is to carry out further investigations of the light curves of β Pic by searching for transit events that can be interpreted as exocomet passages across the star's disk based on data from sectors 32, 33, and 34, which were observed by TESS recently.

2. The TESS β Pic data collection

The Mikulski Archive for Space Telescopes (MAST) contains observations of β Pic collected by TESS from 19 October 2018 to 8 February 2020. TESS observed β Pic in seven sectors, that is to say 4, 5, 6, 7, 32, 33, and 34, covering a period of 844 days. To analyze the β Pic brightness variations, we used the 2-min "short" cadence presearch data conditioning (PDC) light curves produced by the science analysis pipeline of the Science

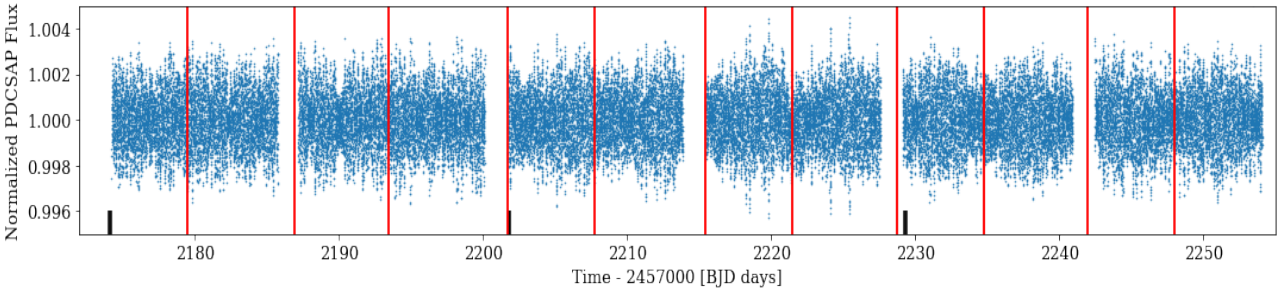

Fig. 1. Stitched light curve of β Pic from sectors 32, 33, and 34. The beginning of each sector is marked with a black vertical line. The red lines mark momentum dumps when angular momentum was removed from the spacecraft reaction wheels, and the spacecraft stability decreased for 10–15 min.

Processing Operation Center (SPOC; Jenkins 2017). The PDC segment of the SPOC performs a set of corrections to the light curves by removing the instrumental signatures and isolated outliers, as well as by correcting fluxes for the aperture effects such as field crowding or fractional loss of the target flux due to star centroid drifting (Jenkins et al. 2016). In general, we used the algorithm for the light curve analysis based on the Python package "LIGHTKURVE V2.0" (Barentsen et al. 2019; Lightkurve Collaboration 2018), which is partially similar to that thoroughly described in Zieba et al. (2019). To assess the available data, we downloaded the fits files from the MAST archive containing the PDC fluxes, centroid measurements, and the "quality flags" information. The latter was used to check the possible influence of different anomalies on the flux measurements[1]. Figure 1 shows the stitched light curves for the data set stored in sectors 32, 33, and 34. The black vertical lines show the beginning of each sector. The gaps in the light curves are caused by the science data downloading process carried out at each perigee during the 18–24 h when no science data were collected. The red lines mark momentum dumps when the angular momentum was removed from the spacecraft reaction wheels, and the spacecraft stability decreased for 10–15 min[2]. The data in the vicinity of the momentum dumps were omitted from the analysis.

3. Data analysis and results

3.1. Identification and removal of pulsations from the β Pic light curve

β Pic belongs to a group of δ Scuti variable stars with significant periodicities in its light curve (see Koen 2003; Zwintz et al. 2019, and references therein). Therefore, we removed the harmonic content from the input signal prior searching for the comet-like signatures. Zieba et al. (2019) identified up to 54 significant p-modes between 23 and 76 cycles per day, applying iterative fitting of the TESS β Pic light curves by superposition of sine-waves extracted with the PERIOD04 program (Lenz & Breger 2005). It is worth noting that the identification and subsequent removal of phase-shifting harmonics from the light curves represent one of the tasks of the Transit Planet Search (TPS) segment of the science analysis pipeline, and the whitened light curves are provided for each 2-min cadence light curve and stored in the MAST archive. The sophisticated whitening algorithms considerably simplify the transit search; however, they distort the transit shape (Thompson 2016). Therefore, to avoid any degrading of the potential asymmetric dips in the light curves due to overfitting, we conducted the extraction of the harmonic signal from the light curves for each sector separately using the Python package SMURFS, which is designed to identify and remove significant frequencies from a time series in a fully automated way[3]. Thus we modeled the light curves for each sector by superposition of the pulsation frequencies between 20 and 80 cycles per day and with the amplitudes down to 0.02 mmag. For sector 6, for example, the frequencies with a signal-to-noise ratio (S/N) ≥4.5 were confidently identified and consistent with those extracted by Zieba et al. (2019) (see Table B.1). Figure 2 presents the differences between the observed and modeled light curves for sectors 5, 6, 32, 33, and 34 observed by TESS. For sectors 5 and 6, we also depict the residual fluxes taken from Zieba et al. (2019) in order to show that applying the two different software packages, that is to say PERIOD04 and SMURFS, to model light curves results in identical residual signals. The black lines mark the minima found in the light curves, likely associated with the transits. There are no notable dips in sector 34 which the dimming events could cause. In the bottom panel of Fig. 2, we depict the flux differences between the modeled and observed light curves of sector 34 to show that they fall in the interval ± 0.2 mmag.

3.2. Confirmation of the known comet transits.

After removing the harmonic content from the signals, we averaged the flux within 30 min bins for each sector separately and smoothed the binned light curves with the Savitzky-Golay filter. Smoothing minimizes noise due to remnants of the star variability while maintaining the depth of the transits. Figure 3 depicts the previously found minima by Zieba et al. (2019) in the light curves observed in sectors 5 and 6 in the same plot. The deepest event closely resembles the theoretical prediction of the transit caused by the passage of a comet-like body across a stellar disk (Lecavelier Des Etangs et al. 1999). The transit duration (from the beginning of the steep brightness fall to the interception with the 1.0 flux line at the transit egress) and its manually measured depth are 2.01 ± 0.03 day and 0.99814 ± 0.00005, respectively, which is in agreement with results presented by Zieba et al. (2019). The transit profiles depicted in Fig. 3 show that the normalized fluxes at the transit ingresses surpass the fluxes at the egresses for all three events. It is consistent with the conclusion of Zieba et al. (2019) on the presence of the "long-lived forward scattering halo" associated with the deepest event, and we argue that it can also be seen in the profiles of the two other small dips.

[1] http://archive.stsci.edu/missions/tess/doc/TESS_Instrument_Handbook_v0.1.pdf
[2] https://archive.stsci.edu/tess/tess_drn.html
[3] https://github.com/MarcoMuellner/SMURFS

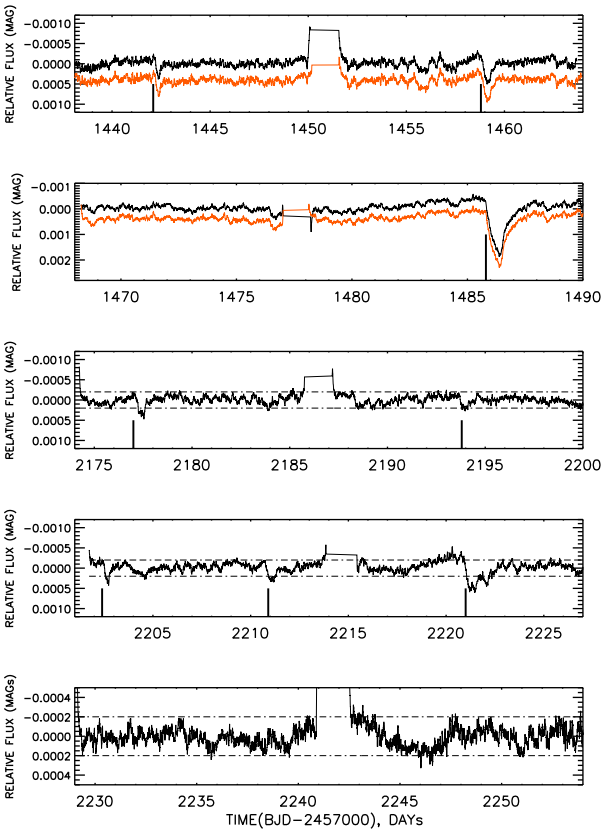

Fig. 2. Differences between the model and observed light curves of β Pic for sectors 5, 6, 32, 33, and 34 (*from top to the bottom*, respectively). The black and orange curves in the two top panels display the light curve residuals obtained in this work and by Zieba et al. (2019), respectively. A small offset was applied for clarity.

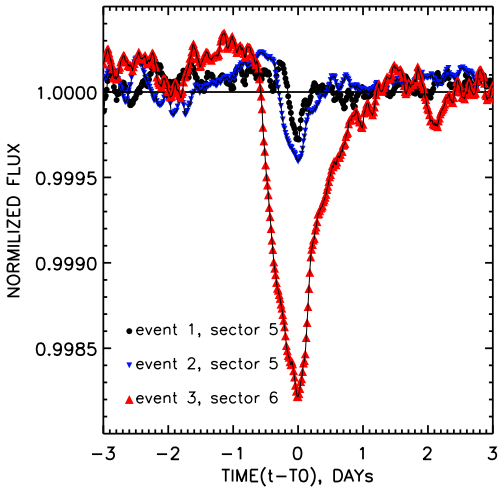

Fig. 3. Asymmetric dips previously found in the TESS PDC light curves of β Pic in sectors 5 and 6 (Zieba et al. 2019). Time is shown relative to the moments of flux minima T_0 = 1442.37 ± 0.02 BJD, 1459.16 ± 0.02 BJD, and 1486.40 ± 0.01 BJD for events 1, 2, and 3, respectively.

3.3. New comet transits

Five new asymmetric nonperiodic minima in the β Pic light curve were identified in sectors 32 and 33. The shapes of the dips are similar to those shallow features observed in sector 5. Meanwhile, the light curve downloaded from sector 34 is featureless.

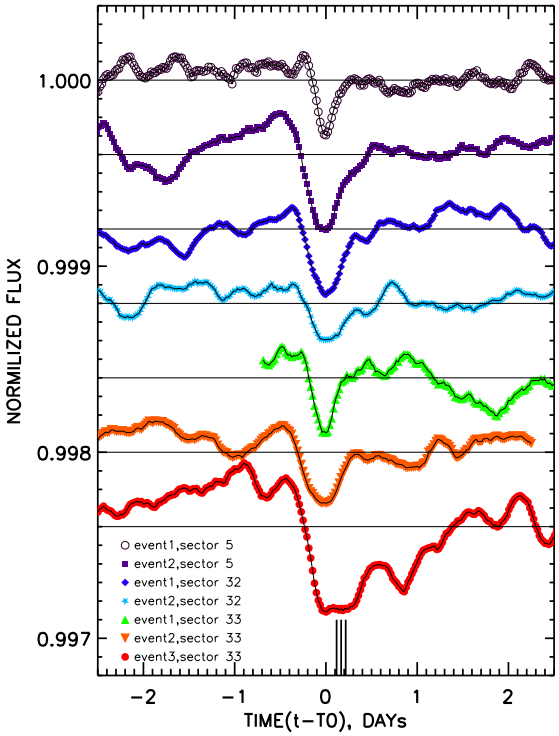

Fig. 4. Asymmetric dips previously discovered in the TESS PDC light curves of BP in sector 5 (Zieba et al. 2019), as well as new ones discovered in sectors 32 and 33. An offset of 0.0004 was applied on the flux values for clarity. Time is shown relative to the moments of the flux minima T_0: for events 1 and 2 in sector 5, T_0 is the same as in Fig. 3; T_0 = 2177.45 ± 0.03 BJD and 2193.98 ± 0.02 BJD for events 1 and 2 in sector 32, and T_0 = 2202.71 ± 0.02 BJD, 2211.11 ± 0.01, and 2221.4 ± 0.1 BJD for events 1, 2, and 3 in sector 33, respectively.

Figure 4 shows the profiles of new events in sectors 32 and 33, along with the previously observed ones in sector 5 for comparison. The first dip detected in sector 33 occurred at the beginning of the sector (the minimum corresponds to the Barycentric Julian date, BJD, T_0 = 2202.71 ± 0.02) so this light curve in the figure is truncated from the left. We estimated the duration and depth of all dips with manual measurements of the time span between the ingress and egress points on the smoothed light curves presented in Figs. 3 and 4. The measured duration values are listed in Table 1 (see Sect. 3.3). All weak dips are very shallow at level of 0.03% with a duration between 0.5 and 0.9 days. The only exception is the last event identified in sector 33, which is not reliable because it partially overlaps with the spacecraft's coarse pointing due to the momentum dump: the transit ingress starts at approximately 2220.74 BJD, the flux minimum occurs at approximately 2221.4 BJD, and the momentum dump event covers the time span between 2221.46 and 2221.47 BJD. To verify the reliability of the data from sectors 32 and 33, we examined the instantaneous row and column positions of the target's flux-weighted centroids in the CCD frames. This information is available for each 2-min cadence PDCSAP light curve. Additionally, we looked through TESS Data Release Notes on sectors 32 and 33, which contain information about observation circumstances, notes on individual targets, spacecraft pointing, data anomalies, etc.[4]. Figure 5 shows the position drift of the flux-weighted centroids with time. The black rectangles mark the identified transit events, the red dashed lines mark coarse spacecraft pointing, mainly due to

[4] https://archive.stsci.edu/tess/tess_drn.html

Table 1. Fitting parameters from MCMC.

Sector	T_0	g	$C_e \times 10^3$	$1000/\lambda$, 1 rad^{-1}	P, days	V_{circ}, km s^{-1}	a_{circ}, au	T_{dur}, days
5_1	1442.357 ± 0.004	0.9975	1.17 ± 0.14	21.7 ± 7.0	625	30.2 ± 1.0	1.74	0.60 ± 0.05
	1442.425 ± 0.010	0	1.15 ± 0.80	2.4 ± 4.0	151	48.6 ± 11.1	0.68	
5_2	1458.970 ± 0.003	0.9970	1.58 ± 0.07	6.6 ± 0.6	811	27.8 ± 0.4	2.07	1.04 ± 0.05
	1459.020 ± 0.003	0	1.16 ± 0.11	2.5 ± 0.5	360	36.3 ± 1.6	1.21	
6 (*)	1485.919 ± 0.001	0.9950	3.73 ± 0.03	1.23 ± 0.03	2753	18.48 ± 0.08	4.68	2.01 ± 0.03
	1485.947 ± 0.002	0	3.83 ± 0.03	0.99 ± 0.03	2335	19.52 ± 0.14	4.19	
6 (**)	1486.290 ± 0.001	0	3.67 ± 0.04	1.22 ± 0.04	2307	19.6 ± 0.1	4.15	–
32_1	2177.397 ± 0.005	0.9950	1.18 ± 0.05	3.0 ± 0.6	640	30.1 ± 0.9	1.76	0.77 ± 0.11
	2177.498 ± 0.005	0	2.22 ± 0.05	0.7 ± 0.2	481	33.0 ± 0.8	1.46	
32_2	2193.890 ± 0.003	0.9975	1.18 ± 0.11	5.5 ± 1.0	735	28.7 ± 0.8	1.94	0.85 ± 0.05
	2193.920 ± 0.005	0	0.94 ± 0.30	1.2 ± 0.9	441	34.0 ± 3.1	1.38	
33_1	2202.646 ± 0.003	0.9700	0.76 ± 0.03	15.1 ± 1.8	124	52.0 ± 1.5	0.59	0.51 ± 0.04
	2202.673 ± 0.003	0	0.99 ± 0.10	4.8 ± 1.1	106	54.8 ± 2.8	0.53	
33_2	2210.931 ± 0.003	0.9800	0.50 ± 0.01	5.5 ± 0.5	743	28.6 ± 0.6	1.95	0.67 ± 0.02
	2210.947 ± 0.006	0	0.47 ± 0.03	9.5 ± 5.8	252	41.0 ± 5.5	0.95	
33_3 (***)	2221.416 ± 0.004	0.9955	1.19 ± 0.02	5.0 ± 0.3	1802	21.3 ± 0.2	3.53	1.76 ± 0.13
	2221.510 ± 0.003	0	0.80 ± 0.02	3.2 ± 0.4	918	26.6 ± 0.2	2.25	

Notes. Indices at the sector number in the first column specify the event number. T_{dur} is an event duration which was measured manually. The first line of each transit contains model parameters if a scattering function is included in the model, and the second line contains model parameters if scattering is not taken into account. (*)This work. (**)Zieba et al. (2019). (***)Degraded by the momentum dump.

the momentum dumps (solid black lines), and the green dash-dotted lines show flares in the frames, which can degrade the background signal. Although the last event overlaps with the spacecraft's coarse pointing period due to the momentum dump, the centers of the star centroid did not shift significantly on the CCD detector (≤0.01 pixel, negligible compared to the aperture size) to cause the fractional loss of the target flux.

3.4. Modeling of transit events

To model exocomet transits, we followed the procedure described in Brogi et al. (2012) and Zieba et al. (2019). In fact, in our computation, we used the modification of the Python code uploaded to GitHub by Zieba et al. (2019)[5]. Bellow we provide some information about the main steps and essential features of the model calculations.

We assumed a circular comet orbit with period P orbiting the star of mass M and radius R. For β Pic, we adopted $M_{star} = 1.80\,M_{Sun}$ and $R_{star} = 1.53\,R_{Sun}$ (Wang et al. 2016). The light curves with removed oscillations by the SMURFS package were used in our analysis. We compared our cleaned light curves with the light curves reduced by Zieba et al. (2019) and found rather marginal differences (see Sect. 3.1).

Zieba et al. (2019) used five parameters (t_{mid}, b, c_e, λ, and P) to optimize the model. Here, t_{mid} marks an arbitrary point along the orbit following the nomenclature of Brogi et al. (2012), but we adopted it as the midpoint of the transit, b is the impact parameter, c_e and $1/\lambda$ are the maximum of extinction cross section and characteristic size scale of the cometary tail, respectively, and P is the orbital period (see Appendix A for more details).

We used the Python routine SCIPY.OPTIMIZE to determine a zero approximation for the input parameter set by the chi square minimization to fit the observed transit profile. The parameter estimates serve as the input set for a Markov-Chain Monte Carlo (MCMC) fit (see below). Following Zieba et al. (2019), we fixed $b = 0$ to avoid degeneration of the solution caused by the free b parameter. In that way, we constrained the range of P and the λ selection.

As noted above, the deepest transit in sector 6 and some of the shallow transits show a higher flux level at their ingress points compared to the egresses. Therefore, we carried out the fitting procedure for two cases, that is, with and without a scattering function in the model. To account for dust scattering, we used the approach proposed by Brogi et al. (2012), but we did not treat the parameter g ($g \simeq \cos(\varphi)$, where φ is the cone angle in that scattering beam) as a free one, but rather adjusted it iteratively while obtaining the zero approximation set of input parameters. After that, we kept the g parameter fixed and did not include it into the input set for the MCMC fit. To account for scattering, we extended the region of the light curve to which we fit the model up to approximately ±3 days around the t_{mid}.

We used the Python software package EMCEE (Foreman-Mackey et al. 2013) to perform a MCMC fit to the binned light curve around the transit features. The best fit parameters of our model calculations are listed in Table 1 and the transit profiles modeled with the set of the best-fit parameters are also depicted (see Appendix B). We used the orbital periods derived to calculate the orbital axes assuming circular orbits, which are also presented in Table 1 along with the manually measured durations of the transit events.

4. Discussion

The asymmetric shallow dips found in sectors 32 and 33 have a depth and duration similar to those found in sector 5. These drops in the star flux could not be explained by cold spots on the star's surface, as they do not show periodicity connected to the β Pic rotation period (~16 h, $v\sin(i) = 130\,\mathrm{km\,s^{-1}}$, $i \sim 90°$, see Royer et al. 2007) and could not disappear in 1–2 days. It has already

[5] https://github.com/sebastian-zieba/betaPic_comet

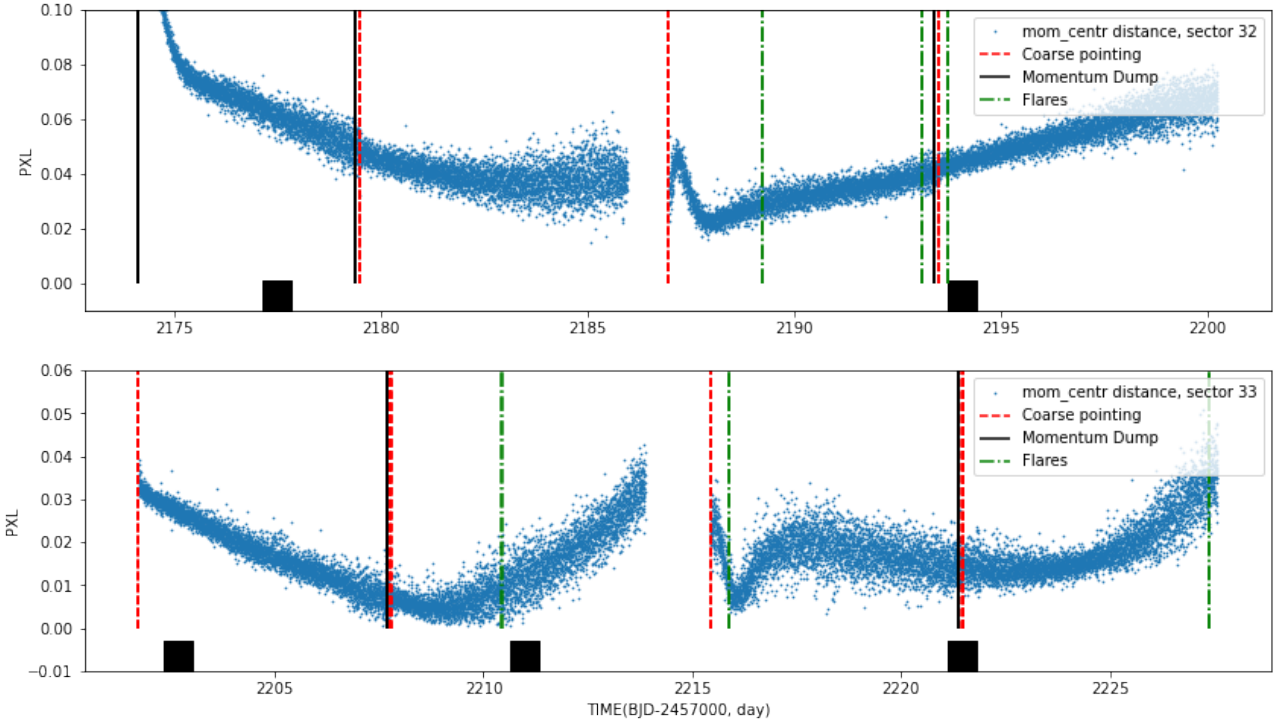

Fig. 5. Instantaneous positions of the target's flux-weighted centroids for sectors 32 and 33. The black rectangles mark the transit events identified. The red vertical dashed lines and black solid lines mark the intervals of the spacecraft's coarse pointing and the momentum dump events, respectively. The green dotted-dashed lines mark flares.

been noted that the brief variations of the β Pic flux were discussed in the context of either a dusty cloud passing over the star disk or an exocomet transit; both explanations seem to be plausible (Lamers et al. 1997). In both cases, the authors consider the contribution of scattering to take into account the brightness spikes before and after the drop of the star flux. In the case of a dusty cloud, the phase function of dust particles can be strongly peaked forward due to diffraction, with the parameter g reaching 0.98 if the cloud is located at a distance larger than 1.5 AU (Lamers et al. 1997). For the newly observed events, the orbital periods obtained with the model allowed us to estimate the distances from the star assuming circular orbits. If the scattering function is not included in the model, the orbital distances of the transiting objects are between 0.5 and 1.5 AU (we do not discuss the last event in sector 33, for which the star flux was degraded by the spacecraft's coarse pointing). Including the scattering function into the model mostly influences the parameter describing the characteristic size scale of the cometary tail, λ, increasing the orbital period and orbital semimajor axis values. Because the scattering function is strongly peaked around the transit midpoint, the model parameters change depending on the g value and transit profile characteristics such as asymmetry relative to the transit midpoint and depth at the flux minimum. According to the model parameters listed in Table 1, the scattering function has a significant impact on the calculated orbital period and circular velocity for events 1 in sector 5 and 2 in sector 33; both of which have slightly shallower profiles than the others.

The parameters extracted for the deepest transit (in sector 6) weakly depend on the scattering function, and in the case of $g = 0$ the model results are in reasonable agreement with those presented in Zieba et al. (2019). For all of the events considered, the increase in the total flux (the star and comet) at the ingress points is approximated by the scattering function with a very high g parameter, pointing out the very narrow scattering that can take place if the medium consists of a mixture of diffracting dusty particles of different sizes (Lamers et al. 1997).

It is also worth noting that several groups can be identified among the β Pic FEB events based on the peculiarities of the spectral features observed (Beust & Morbidelli 2000). These groups consist of bodies that evaporate, likely at different distances from the star. Our findings point out that the deepest and longest events in sector 6 and, possibly, the last one in sector 33 with a duration of about 2 days are caused by bodies orbiting the star at distances larger than at least 2 AU. Meanwhile, the comet-like objects that move closer to the star are responsible for the shallow events.

Rappaport et al. (2018) report the first piece of strong evidence for exocomet transits based on the analysis of the light curves of two F2V stars, KIC 3542116 and KIC 11084727, from the *Kepler* database. Among seven events discovered in the star's light curve, three are very shallow ($\leq$1%) with a duration of less than 1 day. Another star with an exocomet signature is KIC 8462852, whose light curve observed with the *Kepler* mission reveals irregularly shaped aperiodic dips of different depths (Boyajian et al. 2016). The plausible models to explain the observed light curves invoke circumstellar material spread around a single elliptical orbit or the fragmentation of one massive exocomet into multiple cometary nuclei with slightly different orbits (Boyajian et al. 2016; Bodman & Quillen 2016; Wyatt et al. 2018).

The sporadic drops in the β Pic light curve can also be linked to the phenomenon of "little dippers". They are quasi-periodic or aperiodic minima in the light curves of young stars (less than 10 Myr) or even comparatively old stars without IR excess, which were first discovered in the classical T-Tauri star DF Tau (Chelli et al. 1999). The drops in the light curves have diverse shapes, durations of ~0.5–1 day, and depth of ~0.1–1.0% (see Bodman et al. 2017; Ansdell et al. 2019, and references

therein). Some quasi-periodic variations in the "little dipper" light curves can be explained by a model of the spots on the surface of rotating stars or by extinction caused by optically thick dusty clamps corotating with the star (Bodman et al. 2017). But other irregular dimming events are also consistent with the transit of a comet-like body in a circular or eccentric orbit (Scaringi et al. 2016).

In this paper, we have performed the analysis of light curves of β Pic observed by TESS in seven sectors and detected eight events that spark our interest (see Table 1). Thus, we have an average of one event every 27 days, but their distribution is very uneven. Namely, in the sectors 4, 7, and 34, such events are not observed at all; on the other hand, in sector 33 we found as many as three events. Thus far, we can claim that weak dimming events will be observed more often. It is worth noting that the irregularity of manifestations of related objects (FEBs) has been claimed in some works (see, for example, Beust & Morbidelli 2000), but the frequency of events is much higher, reaching several hundred per year.

5. Conclusions

We independently analyzed the light curves of β Pic observed by the TESS mission to perform a new search for exocomet transits in the recently observed sectors 32, 33, and 34. We do not detect any regular planet transits in the 2 min short cadence light curves. We confirm the existence of the known comet transits detected by Zieba et al. (2019) and report new transit events in sectors 32 and 33.

These new transits have asymmetric profiles with very shallow flux drop at level of 0.03% and a duration between 0.51 and 2.01 days with a measurement uncertainty of 0.03–0.13 days. The newly found transits are very similar in duration and depth to those shallow asymmetric dips (except the last one that is degraded by the spacecraft coarse pointing), which were discovered by Zieba et al. (2019) in sector 5, as well as to those found for KIC 3542116 and KIC 11084727 in the *Kepler* database (Rappaport et al. 2018).

We conclude that the young system of β Pic shows significant comet activity. At least eight events with asymmetrical profiles resembling the shapes of exocomet transits have been detected in a comparatively short time interval of ~850 days, among which at least one deep transit has been detected. In the Solar System, a big comet appeared once in 10–20 yr (see Licht 1999). In the case of β Pic, we provide more evidence for the similarity of the newly discovered transits with the known ones with a depth of less than 0.1%; most likely, it is a common phenomenon.

Acknowledgements. This study was performed in the frames of the government funding program for institutions of the National Academy of Sciences of Ukraine (NASU) and supported by the National Research Foundation of Ukraine (№ 2020.02/0228). The authors gratefully thank to the anomymous Referee for the constructive comments and recommendations which definitely help to improve the readability and quality of the paper. We thank Dr. Sebastian Zieba for his comments and help with the model calculations. All data presented in this paper were obtained from the Mikulski Archive for Space Telescopes (MAST), which is hosted at STScI. STScI is operated by the Association of Universities for Research in Astronomy, Inc., under NASA contract NAS5-26555. Support for MAST for non-HST data is provided by the NASA Office of Space Science via grant NNX09AF08G and by other grants and contracts. This paper includes data collected by the TESS mission. Funding for the TESS mission is provided by the NASA Science Mission directorate. Many thanks to Prof. Hugh Jones (UH, Hatfield) for his help in improving the language of the paper.

References

Ansdell, M., Gaidos, E., Jacobs, T. L., et al. 2019, MNRAS, 483, 3579
Backman, D. E., Gillett, F. C., & Low, F. J. 1986, Adv. Space Res., 6, 43
Barentsen, G., Hedges, C. L., De Miranda Cardoso, J. V., et al. 2019, in American Astronomical Society Meeting Abstracts, 233, 109.08
Beust, H., & Morbidelli, A. 2000, Icarus, 143, 170
Beust, H., Lagrange, A. M., Plazy, F., & Mouillet, D. 1996, A&A, 310, 181
Beust, H., Lagrange, A. M., Crawford, I. A., et al. 1998, A&A, 338, 1015
Bodman, E. H. L., & Quillen, A. 2016, ApJ, 819, L34
Bodman, E. H. L., Quillen, A. C., Ansdell, M., et al. 2017, MNRAS, 470, 202
Boyajian, T. S., LaCourse, D. M., Rappaport, S. A., et al. 2016, MNRAS, 457, 3988
Brogi, M., Keller, C. U., de Juan Ovelar, M., et al. 2012, A&A, 545, L5
Chelli, A., Carrasco, L., Mújica, R., Recillas, E., & Bouvier, J. 1999, A&A, 345, L9
Claret, A. 2000, A&A, 363, 1081
Cote, J. 1987, A&A, 181, 77
Crawford, I. A., Beust, H., & Lagrange, A. M. 1998, MNRAS, 294, L31
Crifo, F., Vidal-Madjar, A., Lallement, R., Ferlet, R., & Gerbaldi, M. 1997, A&A, 320, L29
Ferlet, R., Hobbs, L. M., & Madjar, A. V. 1987, A&A, 185, 267
Foreman-Mackey, D., Hogg, D. W., Lang, D., & Goodman, J. 2013, PASP, 125, 306
Frattin, E., Cremonese, G., Simioni, E., et al. 2017, MNRAS, 469, S195
Henyey, L. G., & Greenstein, J. L. 1941, ApJ, 93, 70
Jenkins, J. M. 2017, Kepler Data Processing Handbook: Overview of the Science Operations Center, Kepler Science Document KSCI-19081-002
Jenkins, J. M., Twicken, J. D., McCauliff, S., et al. 2016, SPIE Conf. Ser., 9913, 99133E
Kalas, P., Larwood, J., Smith, B. A., & Schultz, A. 2000, ApJ, 530, L133
Kiefer, F., Lecavelier des Etangs, A., Boissier, J., et al. 2014, Nature, 514, 462
Koen, C. 2003, MNRAS, 341, 1385
Lagrange-Henri, A. M., Vidal-Madjar, A., & Ferlet, R. 1988, A&A, 190, 275
Lagrange, A. M., Rubini, P., Nowak, M., et al. 2020, A&A, 642, A18
Lamers, H. J. G. L. M., Lecavelier Des Etangs, A., & Vidal-Madjar, A. 1997, A&A, 328, 321
Lecavelier Des Etangs, A., Deleuil, M., Vidal-Madjar, A., et al. 1995, A&A, 299, 557
Lecavelier Des Etangs, A., Vidal-Madjar, A., & Ferlet, R. 1999, A&A, 343, 916
Lenz, P., & Breger, M. 2005, Commun. Asteroseismol., 146, 53
Licht, A. L. 1999, Icarus, 137, 355
Lightkurve Collaboration (Cardoso, J. V. d. M., et al.) 2018, Lightkurve: Kepler and TESS Time Series Analysis in Python
Mamajek, E. E., & Bell, C. P. M. 2014, MNRAS, 445, 2169
Meech, K. J., & Jewitt, D. C. 1987, A&A, 187, 585
Rappaport, S., Vanderburg, A., Jacobs, T., et al. 2018, MNRAS, 474, 1453
Royer, F., Zorec, J., & Gómez, A. E. 2007, A&A, 463, 671
Scaringi, S., Manara, C. F., Barenfeld, S. A., et al. 2016, MNRAS, 463, 2265
Smith, B. A., & Terrile, R. J. 1984, Science, 226, 1421
Thompson, S. E. 2016, Data Validation Time Series File: Description of File Format and Content, Kepler Science Document KSCI-19079-001
Wahhaj, Z., Koerner, D. W., Ressler, M. E., et al. 2003, ApJ, 584, L27
Wang, J. J., Graham, J. R., Pueyo, L., et al. 2016, AJ, 152, 97
Wyatt, M. C., van Lieshout, R., Kennedy, G. M., & Boyajian, T. S. 2018, MNRAS, 473, 5286
Zieba, S., Zwintz, K., Kenworthy, M. A., & Kennedy, G. M. 2019, A&A, 625, L13
Zuckerman, B., & Song, I. 2004, ARA&A, 42, 685
Zwintz, K., Reese, D. R., Neiner, C., et al. 2019, A&A, 627, A28

Appendix A: Comet transit modeling formulae

To calculate the theoretical profiles, we used the model described by Brogi et al. (2012) and adapted by Zieba et al. (2019). It is considered that a comet moves on a circular orbit; readers can refer to Fig. 4 in Brogi et al. (2012) for more geometric details.

The total flux as a function of orbital phase φ is

$$I(\varphi) = \frac{1}{\delta}\int_{2\pi\varphi-\delta/2}^{2\pi\varphi+\delta/2}[1 - I_e(\theta) + I_s(\theta)]d\theta,$$

where I_e and I_s are the contributions of the extinction and scattering components, respectively. We would like to note that $\varphi = 2\pi\theta$, where θ is the angle between the observer, the center of the star, and the orbiting body. Furthermore, $\delta = 2\pi\Delta t/P$, where Δt is the exposure time and P is the comet's orbital period.

The extinction component is expressed as

$$I_e(\theta) = \int_0^{2\pi}\rho(\theta - \theta')i(\theta', \hat{r}_c)d\theta',$$

where $\theta - \theta' = \Delta\theta$ is the angular distance between the position of the comet and the arbitrary point along the orbit (in this work, θ' marks the midpoint of the transit event).

The model assumes an optically thin cometary coma expressed in units of the stellar area and its extinction cross section ρ drops exponentially away from the center as

$$\rho(\Delta\theta) = \frac{\rho_0}{\pi R_\star^2}e^{-\lambda(\Delta\theta)} \equiv c_e e^{-\lambda(\Delta\theta)},$$

where the multiplicative factor, c_e, and the exponential parameter, λ, are free parameters of the model.

The chord length that a comet traverses in the stellar disk is represented by the impact parameter $b = [1 - (r_c/2R_\star)^2]^{1/2}$. The angle of the crossed chord as seen from the comet orbit is given by $\hat{r}_c = \arcsin(r_c/2a)$. Here, $R_\star$ and a are the stellar radius and the orbital radius of the comet, respectively. The latter is calculated from the orbital period.

The extinction component is the convolution between the extinction cross section and the intensity of the stellar disk. The latter one, in terms of θ' and $\hat{r}_c$, is given by

$$i(\theta', \hat{r}_c) = 1 - u\left[1 - \frac{a}{R_\star}\sqrt{\sin^2(\hat{r}_c/2) - \sin^2\theta'}\right],$$

where u is the linear limb-darkening coefficient, which we adopted as 0.79 (Claret 2000).

The scattering component $I_s(\theta)$ is given by

$$I_s(\theta) = \pi\varpi\left(\frac{R_\star}{a}\right)^2\int_0^{2\pi}\rho(\theta - \theta')\bar{p}(\theta')d\theta',$$

where $\bar{p}(\theta')$ is the Henyey-Greenstein (H-G) phase function (Henyey & Greenstein 1941)

$$\bar{p}(\theta') = \frac{1 - g^2}{4\pi(1 - 2g\cos\theta' + g^2)^{\frac{3}{2}}}.$$

The parameter g is the asymmetry parameter in the range between -1 and 1, with $g > 0$ and $g < 0$ for forward-peaked and backward-peaked scattering functions, respectively, and ϖ is the single-scattering albedo. We fixed the latter parameter at 0.15, taking into account the estimation of single-scattering albedo values for the solar system comets and assuming a cometary coma as a mixture of volatile and solid dusty components (Meech & Jewitt 1987; Frattin et al. 2017).

Appendix B: Modeled exocometary transits in the β Pic system

This appendix contains the binned β Pic light curves limited to approximately $\pm$ 3 days around the transit events, which were used for the model calculation of the transit profiles with MCMC. For each transit, the model profile calculated with the set of the best-fit parameters is also depicted. The left panel of each figure presents the modeled light curve if the scattering function is not included in the model, whereas the right panel shows the transit profile if scattering is taken into account. The sector in which the event occurs as well as the event number are specified in the figure caption. The bottom panels depict residuals.

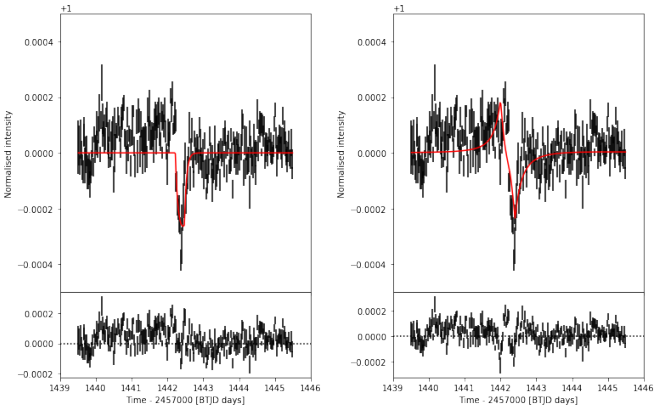

Fig. B.1. Light curve of β Pic limited to approximately $\pm$ 3 days around the transit event 1 in sector 5. The observed and modeled flux are marked with black and red lines, respectively. The upper left panel presents the modeled transit profile in case scattering is not accounted for; the upper right panel shows the modeled transit profile in case the scattering function is included into the model. The bottom panels show residuals between the observed and modeled flux.

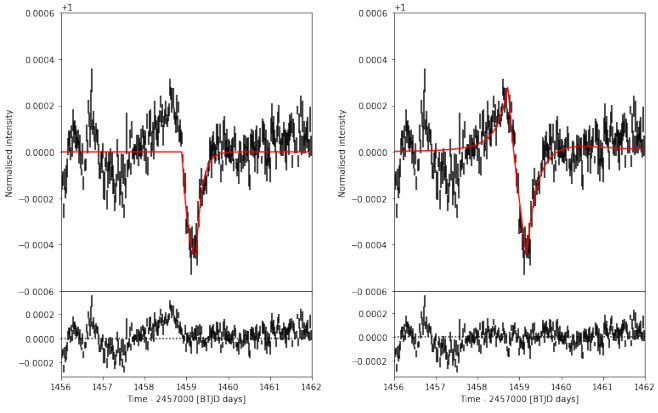

Fig. B.2. Same as Fig. B.1, but for event 2 in sector 5.

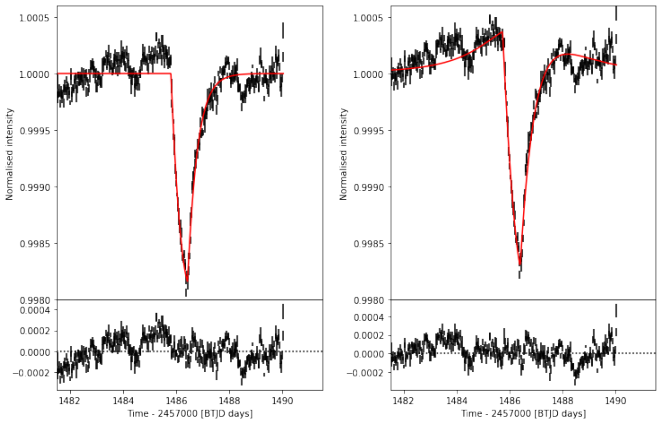

Fig. B.3. Same as Fig. B.1, but for transit in sector 6.

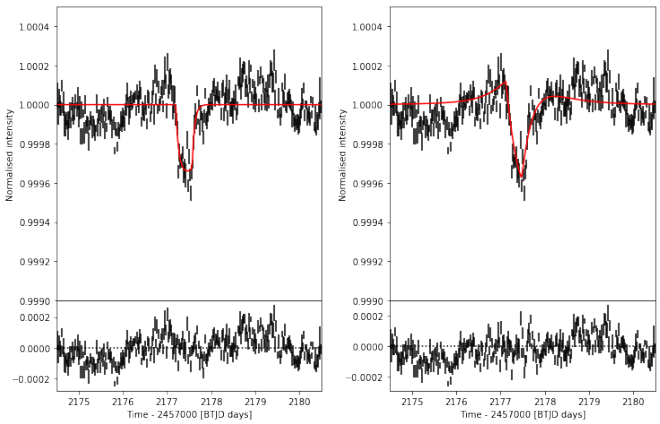

Fig. B.4. Same as Fig. B.1, but for event 1 in sector 32.

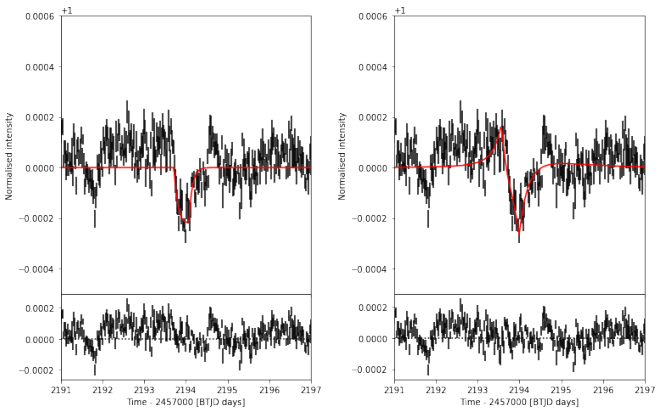

Fig. B.5. Same as Fig. B.1, but for event 2 in sector 32.

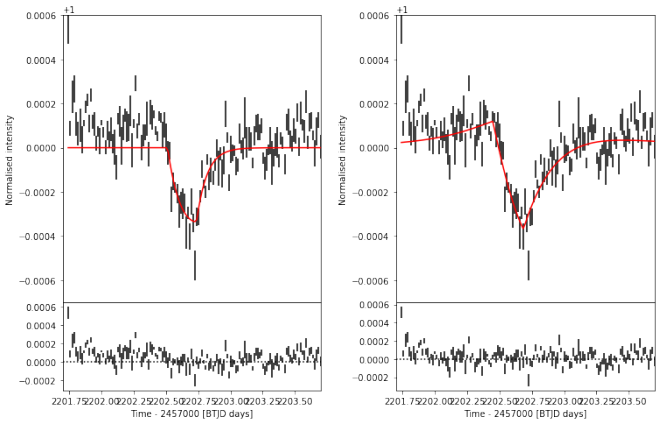

Fig. B.6. Same as Fig. B.1, but for event 1 in sector 33.

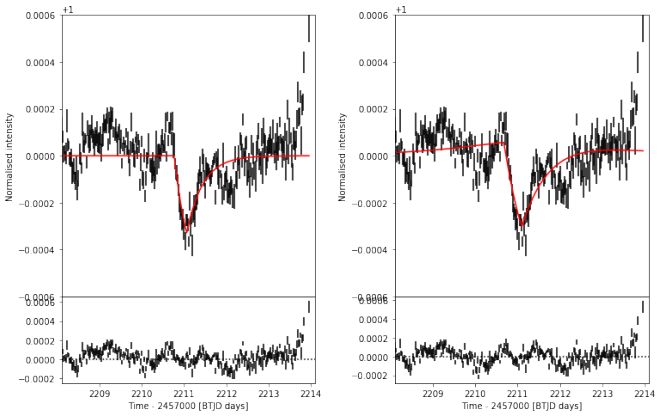

Fig. B.7. Same as Fig. B.1, but for event 2 in sector 33.

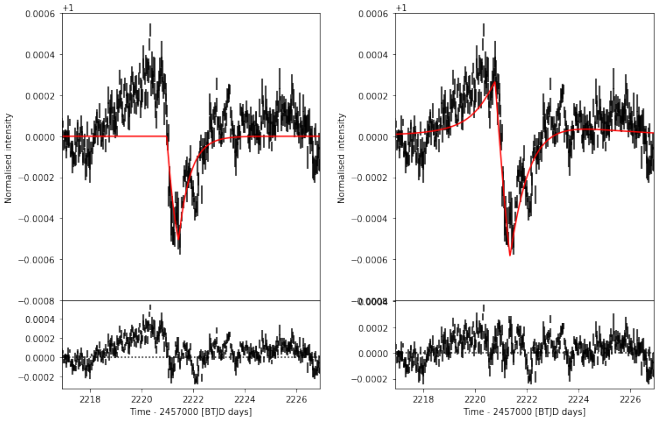

Fig. B.8. Same as Fig. B.1, but for event 3 in sector 33.